Mineral and chemical changes of sediments after Cu sorption and then desorption induced by synthetic root exudate

Hussein Jaafar Kanbar, Malak Kaouk

Mineral and chemical changes of sediments after Cu sorption and then desorption induced by synthetic root exudate

Hussein Jaafar Kanbar [a, b, c *] and Malak Kaouk[a]

[a] Applied Plant Biotechnology Laboratory (APBL). Faculty of Sciences, Department of Earth and Life Sciences. The Lebanese University, Rafic Hariri Campus, Hadat, Lebanon.

[b] Research and Analysis Platform for Environmental Sciences (PRASE), Doctoral School of Sciences and Technology (EDST). Faculty of Sciences. The Lebanese University, P.O. 5, Rafic Hariri Campus, Hadat, Lebanon.

[c] Department of Chemistry, Umeå University, SE-901 87, Umeå, Sweden.

* Corresponding author: Hsen.kanbar@gmail.com

Graphical Abstract

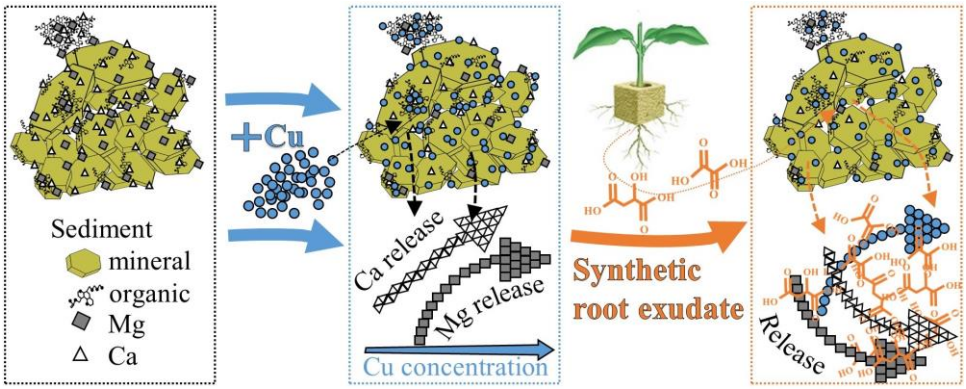

Abstract

Understanding the fate of anthropogenically introduced copper in sediments is important to comprehend the biogeochemical processes; consequently, beneficial utilization of Cu-rich materials can be proposed (e.g. soil amendment). Therefore, we address the behavior of copper and other metals at the liquid-solid interface of different grain sizes in lake sediments. Initially, the sediment fractions were characterized for mineralogy (XRD), chemical structure (FTIR),

physicochemical parameters (mainly pH, cation exchange capacity, and electric conductivity), organic content, and chemical composition (AAS). Then, solutions of varying Cu concentrations were added to the fractions; the Cu concentrations of the sorption experiment were chosen according to the exchangeable cations of each fraction. A desorption experiment by synthetic root exudate was followed. The physicochemical parameters, functional groups, and mineralogy were noted before and after the two experiments. The sorption and desorption of Cu, Ca, Mg, K, and Na were also studied. The sediment fractions had similar mineralogy and chemical structure, yet the physicochemical composition and metal contents were different. The Cu sorption experiment showed that surface Ca and embedded Mg were the main cations that were exchanged with Cu, as shown by linear and logarithmic trends, respectively. The copper-sediment interaction mainly occurred at the organic interface. Finally, synthetic root exudate was able to restore part of the initial chemical structure of the sediments, indicating exchangeable Cu sorption on the organic part of the sediments. The various grain sizes had an insignificant influence on the behavior of metal sorption and desorption.

Keywords: sediment, grain size, copper, sorption, desorption, synthetic root exudate

1. Introduction

Copper is mainly introduced into the environment by Cu mining and smelting, waste incineration bottom ash, vehicular combustion, production of Cu containing nanomaterials, and the application of fertilizers and pesticides (e.g. Azzi et al., 2017; Lee et al., 2008; Seniunaite and Vasarevicius, 2017). Sediments often act as the ultimate sink for metals in the environment (Ammar et al., 2015; Grabowski et al., 2011). Therefore, it is important to understand Cu-sediment interaction. Complex processes are involved in metal-sediment interactions, such as exchange, desorption, sorption, complexation, and precipitation. It is well known that the metal-sediment interaction depends on the chemical state of the metal (i.e. speciation) and the

physical and chemical parameters of the matrix (whether liquid or solid), such as pH, redox potential, mineral composition, cation exchange capacity (CEC), ionic strength, particle size, and organic matter (OM) (e.g. Carrillo-González et al., 2006; Du Laing et al., 2009). In aquatic sediments, sedimentation depends on river hydrodynamics, particle size, and composition. Fine particles are generally enriched with metals since they have higher sorption capacity (Acosta et al., 2011; Du Laing et al., 2007). Moreover, Cu is reported to sorb onto clays, carbonates, Mn and Fe oxides, organic matter, and organo-mineral complexes, especially under alkaline pH (e.g. Fariña et al., 2018; Yuan et al., 2013).

Even though Cu exposure can have toxic effects on plants, it is an essential micronutrient. Copper is involved in metabolic processes for normal plant growth (Yamasaki et al., 2008 and articles cited therein). Therefore, controlled amendment of Cu-rich materials in agriculture can improve plant growth (e.g. Ju et al., 2019; Kobaissi et al., 2014). Importantly, plants can manage nutrient availability and limit toxicity by secreting exudates to the rhizosphere. Root exudates help plants to cope with metal stress by stabilizing metals in the rhizosphere or by changing the pH of the matrix (e.g. Badri and Vivanco, 2009).

Therefore, we studied Cu sorption onto different grain sizes of sediments and Cu desorption induced by synthetic root exudate (SRE). The sorption and desorption of Cu were followed by monitoring other metals that are involved in those processes. Additionally, the change in the physicochemical parameters, mineralogy, and chemical composition of the sediment fractions were investigated before and after the experiments. Coupling the Cu-sediment findings to the geochemical properties of the fractions give indications on the fate of Cu in Cu rich media. More importantly, the findings can be used for selective Cu release and beneficial uptake by biota.

2. Materials and Methods

2.1. Sampling site, sediment collection, and treatment

A mass of submerged sediments was collected from the east side of the Qaraaoun reservoir (33°33'14.8"N, 35°42'02.0"E), which is part of the upper Litani River basin and is located in the Beqaa valley of Lebanon. More information about the sampling site is found elsewhere (Ammar et al., 2015; Kanbar et al., 2014). The sediments were wet sieved using the adjacent river water into sizes of 0 – 64 µm, 64 – 250 µm, 250 – 500 µm, and 500 – 2000 µm (S1, S2, S3, and S4, respectively). Wet sieving was done in order to maintain *in situ* sizes (i.e. aggregates and organo-mineral complexes were not broken). To limit chemical or mineralogical modifications of the samples, they were immediately frozen and later freeze-dried. Homogeneous aliquots of the dry samples were then ground for analyses.

2.2. Sedimentary materials: mineralogical, and physicochemical and chemical parameters

The mineralogical composition (by X-ray diffraction, XRD), functional groups (by Fourier transform infrared, FTIR), cation exchange capacity, pH, electric conductivity (EC), salinity, total dissolved solids (TDS), zeta potential, organic matter, and metal contents were determined for each sediment fraction. The fractions showed similar mineralogy and functional groups (Figure 1). Moreover, the coarsest fraction had the highest organic matter and metal contents, emphasizing the influence of organo-mineral complexes in metal enrichment (detailed information about the methodology and results is included in Supplementary material SM 1).

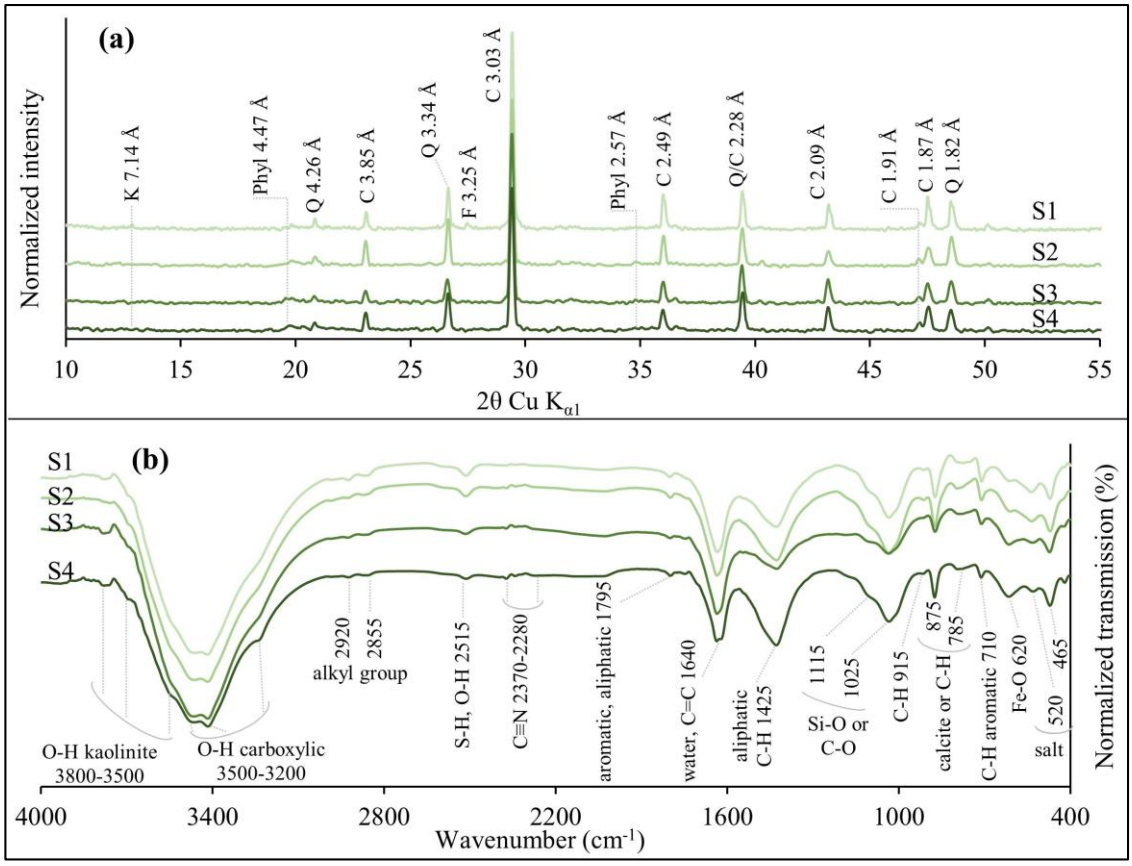

Figure 1: The XRD patterns (a) and the FTIR spectra (b) of the sediment fractions.

a) K: Kaolinite, Phyl: phyllosilicates, Q: quartz, C: calcite, and F: feldspar. The interplanar distances (in Å) and the minerals are assigned to the peaks. b) The functional groups and the wavenumbers (in cm^{-1}) are assigned to the peaks.

S1: 0 – 64 µm, S2: 64 – 250 µm, S3: 250 – 500 µm, and S4: 500 – 2000 µm.

2.3. Copper sorption onto different sediment sizes and consequent changes

Sorption experiments were conducted to study the Cu-sediment binding mechanisms, the consequent cation release or exchange, and the change in physicochemical, mineralogical, and chemical parameters. 50 ml solutions of known Cu concentrations were added to 500 mg of the sediment fractions and mixed for 24 hours under ambient room temperature. The Cu concentrations used in the sorption experiment are equivalent to the CEC values of each fraction. Therefore, the solutions used for each fraction contain different Cu concentrations (SM 2). The Cu concentrations are considered as treatments and are termed C1, C2, C3, C4,

and C5 for the concentrations of Cu equivalent to 0.5CEC, 1CEC, 2.5CEC, 5CEC, and 10CEC, respectively. Each sample was run as four replicates (n=4). Additionally, duplicate negative controls (sediments mixed with ultrapure water, n=8) and positive controls (Cu solutions without sediments, n=20) were prepared and run along with the samples. Electric conductivity and pH values were recorded for the initial solutions (pH_i and EC_i) and after 24 hours (pH_f and EC_f); the final measurements were taken after the solutions were filtered over a 0.45 µm filter. The filtered solutions were also used to quantify Cu, Ca, and Mg by AAS and K and Na by flame photometry. The equilibrium uptake (qe) of Cu was calculated according to the following equation:

$$qe_{(mg/g)} = \frac{(C_i - C_f)_{(mg/L)} \times V_{(L)}}{m_{(g)}}$$

where qe is the equilibrium uptake of Cu (in mg/g), C_i and C_f are the initial and final concentrations of Cu in the solutions (in mg/L), respectively, V is the volume of the sorption solutions (in L), and m is the mass of the sediments (in g). After the sorption experiment, the surface charge (zeta potential, as duplicates), functional groups (FTIR), and mineralogy (XRD) were determined for one sample out of each quadruplicate. The remaining triplicates were used for the Cu desorption experiment.

2.4. Copper desorption induced by synthetic root exudate and consequent changes

The fate of the sorbed Cu from the sorption experiment was followed after mixing with SRE. The SRE components and their concentrations depend on several factors, such as soil type, soil physicochemical conditions (e.g. pH, redox potential, and temperature), nutrient deficiency, metal toxicity, microbiome, plant species, and plant stage of development (e.g. Badri and Vivanco, 2009; Grayston et al., 1997). The SRE components and concentrations used in this study are mainly based on Huang et al. (2017). The concentrations of the compounds are included in SM 3. However, 1 ml of the prepared SRE and 49 ml

ultrapure water were added to each sample from the previous experiment (i.e. a triplicate for each treatment). The mixtures were rotated for 24 hours. Similar to the sorption experiment, the pH and EC values were recorded, the desorbed metals were quantified, and the functional groups and mineralogy were determined.

3. Results and Discussion

3.1. Cu sorption onto sediment fractions

3.1.1. Change in physicochemical parameters

The final EC values (i.e. EC_f) were higher than the initial ones in most cases, such as S1C1-C2 and S2C1-C4 (Figure 2a); this is explained by the cation exchange or release induced by Cu or by the dissolution of sedimentary phases. However, some EC_f values were lower than EC_i, such as S1C3-C5 and S2C5. Even though the high Cu concentrations of the solutions cause the exchange or release of cations, some of those cations might have precipitated, as suggested by $EC_f < EC_i$. Nonetheless, the variation in EC showed a clear and increasing trend with increasing Cu concentrations .

The pH_i values were different for the solutions used in the sorption experiment. Moreover, the variation between pH_i and pH_f (i.e. ΔpH; $\Delta pH = pH_f - pH_i$) was generally prominent for the lower concentrations in the cases of S1, S2, and S4 (mainly C1 in Figure 2b). The pH_i and pH_f values are included in SM 4. Sediments naturally buffer the pH, nonetheless, high Cu concentrations overwhelmed the buffering capacity to some extent, which lead to a drop in the final pH (ΔpH generally decreases from C1 to C5). Furthermore, S4 showed the least variation in ΔpH for all the treatments (C1-C5), possibly linked to the low buffering capacity due to the relatively low Ca contents and carbonates (SM 1).

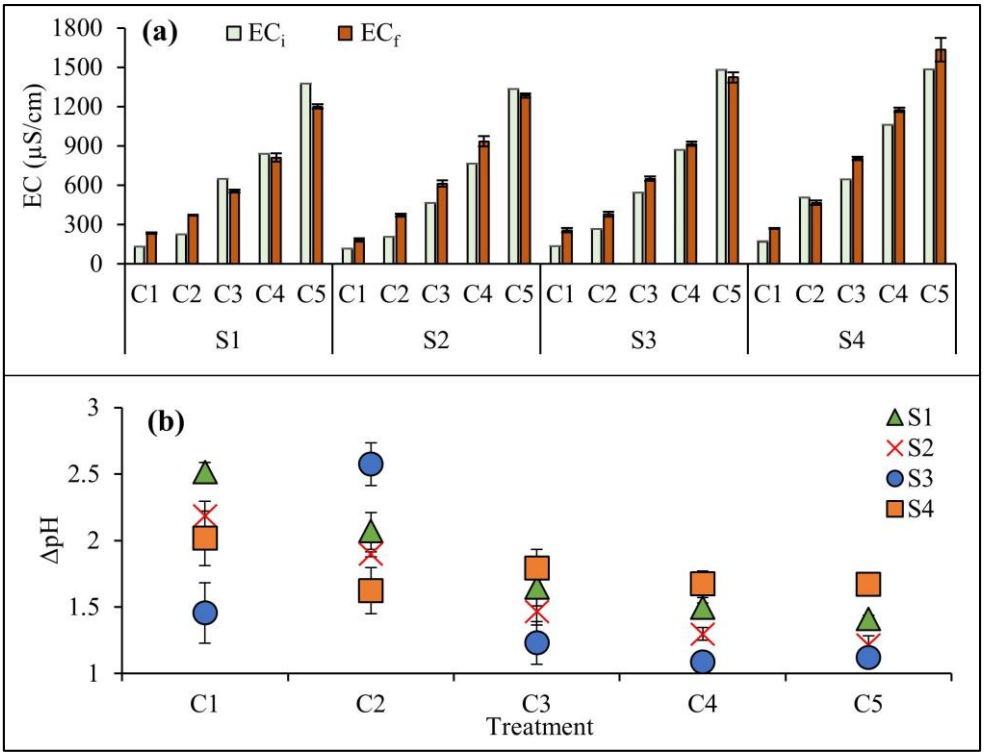

Figure 2: The variation of a) EC (µS/cm) and b) ΔpH (pH_f–pH_i) for the different grain sizes treated with solutions having different Cu concentrations. Whiskers indicate standard deviations of the technical quadruplicates.

S1: 0 – 64 µm, S2: 64 – 250 µm, S3: 250 – 500 µm, and S4: 500 – 2000 µm. For the values of C1 – C5, please refer to SM 2.

141 *3.1.2. Behavior of Cu and other cations*

142 The sediment fractions nearly sorbed 100mg/g of Cu (Figure 3a), which is equivalent to
143 10-fold the CEC; high Cu sorption values (~ 1000 mg/g) are reported in soils and sediments
144 (e.g. Arias et al., 2006; Liu et al., 2015; Ratasuk et al., 2003). Unexpectedly, Cu sorption was
145 identical in all the fractions and 97 to 100% of the added Cu was sorbed after 24 hours (SM 5).
146 The equilibrium uptake of Cu for mainly C5 treatments might be overestimated due to
147 precipitation (see SM 6 for the margin of error). Regression showed a linear fit between Ca
148 release and added Cu concentrations (R^2>0.98 for all fractions; Figure 3b). This direct and

linear relationship suggests that the major exchange between Ca and Cu occurred on the surface. It is worth noting that S4 had the highest Ca release in comparison to the other fractions.

As for Mg release, regression analysis showed a logarithmic fit with the initially added Cu concentrations (Figure 3c), indicating that surface-bound Mg was majorly released when the initial Cu concentrations were low (e.g. C1-2). The decline in Mg release rate with higher Cu concentrations indicates the release of embedded Mg, i.e. Mg absorbed or located in the structure of macropores (Jain and Sharma, 2002). Moreover, Mg release was different for the sediment fractions. It is worth noting that S4 had the highest Ca and Mg release, followed by S3, S2, and finally S1. This trend was also seen for EC (Figure 2a), CEC, and LoI (SM 1). Furthermore, having the highest CEC and Fe and Mn contents (SM 1), S4 is relatively rich in interlayered clay minerals, organic matter, and organo-mineral complexes, which also support the high Ca and Mg release in that fraction (e.g. Jain and Sharma, 2002; K. Li et al., 2018; Q. Li et al., 2018). This further supports that organo-mineral complexes are the key sites for the Cu-cation exchange. According to the trends of Ca and Mg release, Cu mainly competes with Ca and to a lower extent with Mg. Control samples were also run. Due to the absence of a competing cation (i.e. Cu) in the control samples, the release of Ca and Mg were lower than the treated samples. The values for Ca and Mg release in the control samples were 6.8 and 0.7, 5.9 and 0.7, 5.8 and 1.1, and 5.1 and 1.2 mg/L for S1, S2, S3, and S4, respectively (the data are not included in the graphs for clarity reasons). Na and K release did not follow a trend with grain size nor with treatment (SM 7).

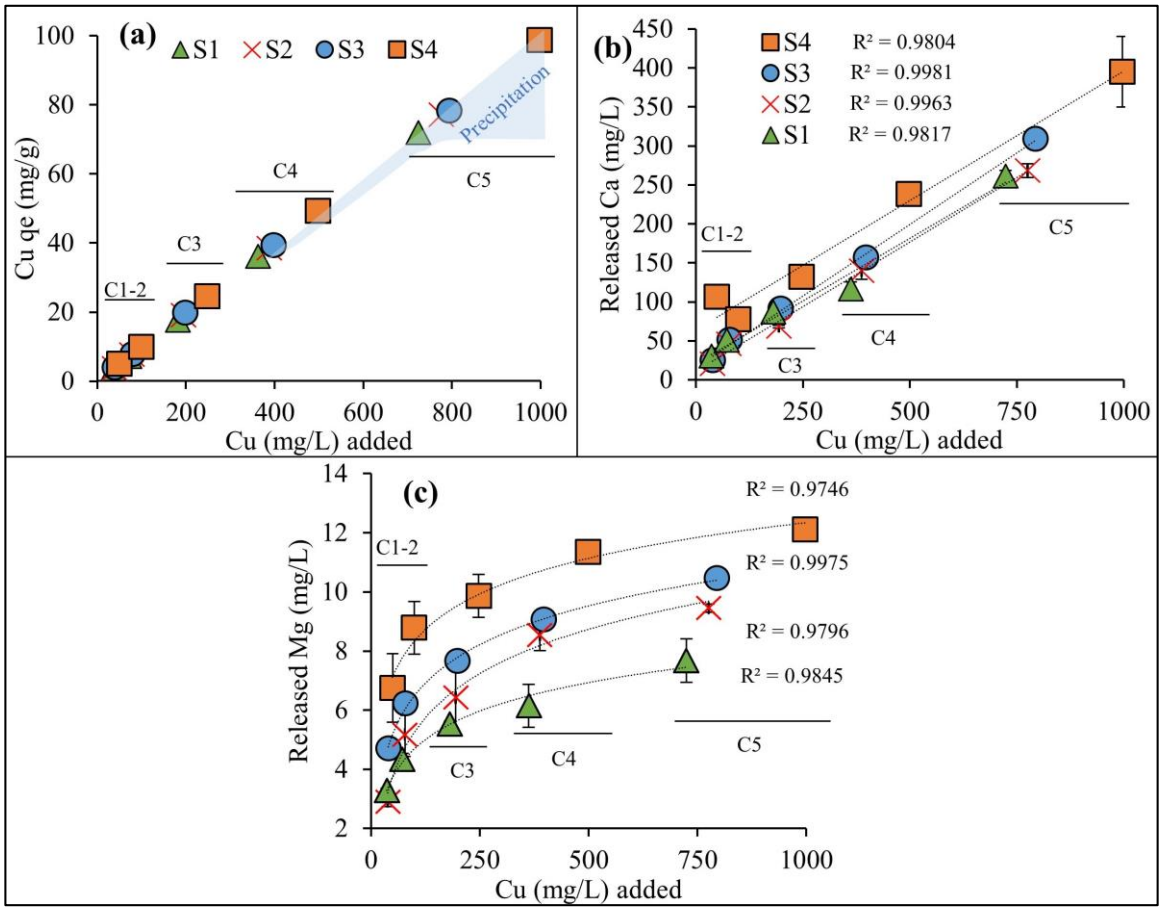

Figure 3: a) The equilibrium uptake (qe) of Cu (mg/g) for the different fractions and treatments; the blue region indicates possible precipitation (SM 6). b) Ca and c) Mg release (in mg/L) for the different fractions and treatments. Whiskers indicate standard deviations of the quadruplicates.

S1: 0 – 64 µm, S2: 64 – 250 µm, S3: 250 – 500 µm, and S4: 500 – 2000 µm.

3.1.3. Mineralogical and chemical changes

In addition to the minerals previously identified in the initial samples (Figure 1a), the XRD patterns showed the protrusion of posnjakite in the C3, C4, and C5 treatments. The intensity of the posnjakite peaks (at 6.98, 3.47, 2.70, and 2.41 Å) increased from C3 to C5 (the example of S3 is given in Figure 4a). The precipitation of this mineral might explain the decline of EC in some samples after Cu sorption (e.g. S1C3-C5 in Figure 2a). Indeed, the experimental

conditions in the sorption experiment, i.e. mixing, temperature, and increase in pH (ΔpH>0), are adequate to produce posnjakite (Zaffino et al., 2015; Zittlau et al., 2013).

Even though the XRD patterns identified posnjakite in samples that underwent C3 – C5 treatments, the FTIR spectra showed this mineral in all the treatments (Figure 4b). Even though it is not possible to indicate what percentage of Cu sorbed onto the sediments and what percentage precipitated, it is well known that Cu sorption starts rather instantly (e.g. Al-Qunaibit et al., 2005; Liu et al., 2015; Veli and Alyüz, 2007), while posnjakite forms within 20 minutes (Zittlau et al., 2013). Therefore, Cu sorption is favored. Posnjakite was identified by FTIR based on O-H stretching at 3549, 3405, and 3244 cm^{-1}, v_3 SO_4^{2-} at 1116 and 1069 cm^{-1}, Cu-OH bending at 792 cm^{-1}, v_4 SO_4^{2-} at 605 cm^{-1}, v_2 SO_4^{2-} and Cu-O stretching at 435 cm^{-1}, and by small peaks at 733, 3950 – 3750, and 1700 – 1200 cm^{-1} (Zaffino et al., 2015). Interestingly, the C-O peak at 1025 cm^{-1} decreased after Cu sorption, mainly in S1, S3, and S4 (Figure 4b), which could indicate the binding of Cu to organic matter by forming a covalent Cu-C bond (e.g. Golubeva et al., 2013). Indeed, Hossain et al. (2012) reported that the carboxyl group can chelate Cu. This might also explain the change in the O-H carboxylic groups in the 3500 – 3200 cm^{-1} region.

The CH_2 and CH_3 deformation vibrations at 1470 and 1350 cm^{-1} and the C=O (carboxyl) stretching or O-H deformation at 1725 cm^{-1} are attributed to Cu sorption (Chen et al., 2015; Gallé et al., 2004); Cu is highly correlated with the carboxyl and alkyl carbon groups of organic matter (Q. Li et al., 2018). Additionally, Cu can form ternary complexes (Alcacio et al., 2001). The protrusion of the 1725 cm^{-1} peak and the fluctuation in the 1700 – 1200 cm^{-1} region after Cu sorption was detected for all the samples except S4C1. The aliphatic or aromatic group at 1795 cm^{-1} and the bands at 2370 – 2280 cm^{-1} disappeared after Cu sorption (except for S3), suggesting the disruption of these functional groups by the formation of Cu-bonds. Interestingly, in the S3 samples, the peak at 1640 cm^{-1} split into two peaks, a unique

200 deformation was detected at 1725 cm^{-1}, and the peaks at 3549, 3405, and 3244 cm^{-1} (belonging
201 to posnjakite) were relatively more prominent. Finally, the change in surface charge (zeta
202 potential) after Cu sorption is included in SM 8.

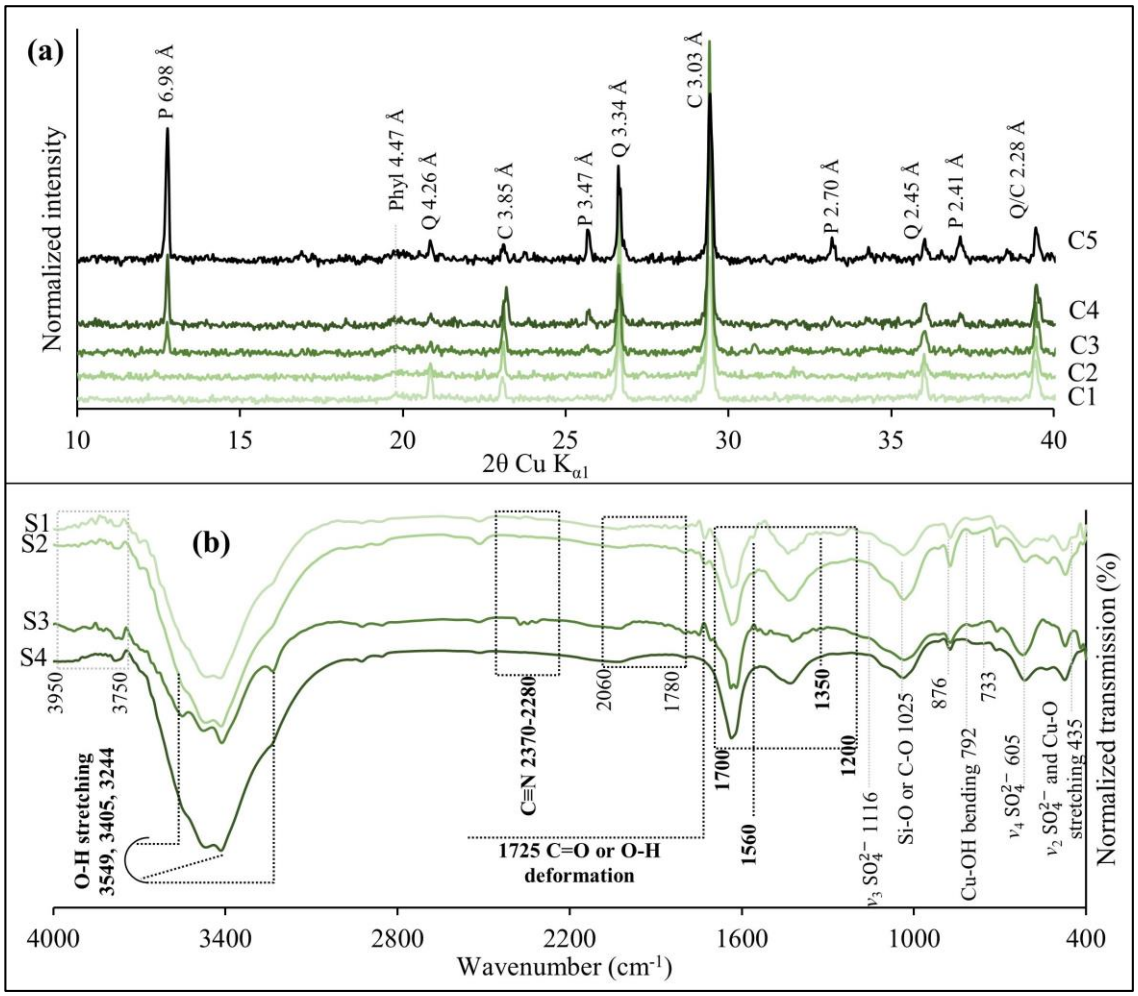

Figure 4: a) XRD patterns showing the protrusion of posnjakite peaks (denoted by P) in the C3 – C5 treatments (example of S3 is given here). b) FTIR spectra after the sorption experiment (example of C1 is given here). The peaks assigned to changes due to Cu sorption are indicated in bold. For the identification of the other peaks, please refer to Figure 1b. S1: 0 – 64 µm, S2: 64 – 250 µm, S3: 250 – 500 µm, and S4: 500 – 2000 µm.

203 **3.2. Cu desorption induced by synthetic root exudate**

204 *3.2.1. Physicochemical changes*

The treatments indicated hereafter denote the different concentrations of Cu that were applied for the Cu sorption experiment; the same SRE solution was used for all the treatments. The pH_f values ranged between 5.7 and 7.5 (Figure 5a). The highest pH change was seen for S4, which also showed the lowest buffering capacity in the sorption experiment. The similar pH_f values for S4C1 and S4C5 indicate that the different Cu concentrations (treatments) in the sorption experiment had similar effects. S2 showed relatively low pH_f values and had a low buffering capacity in the sorption experiment (as seen by a relatively small ΔpH in Figure 2b). As for EC, there was no common trend for the different grain sizes nor for the previously underwent treatments (Figure 5b). The highest EC_f values were recorded for S4, which could be related to the dissolution of carbonates that buffered the pH of the SRE solution from 3.7 to nearly 7.4 (Figure 5a). As for the other fractions, EC fluctuated between 210 and 300 µS/cm.

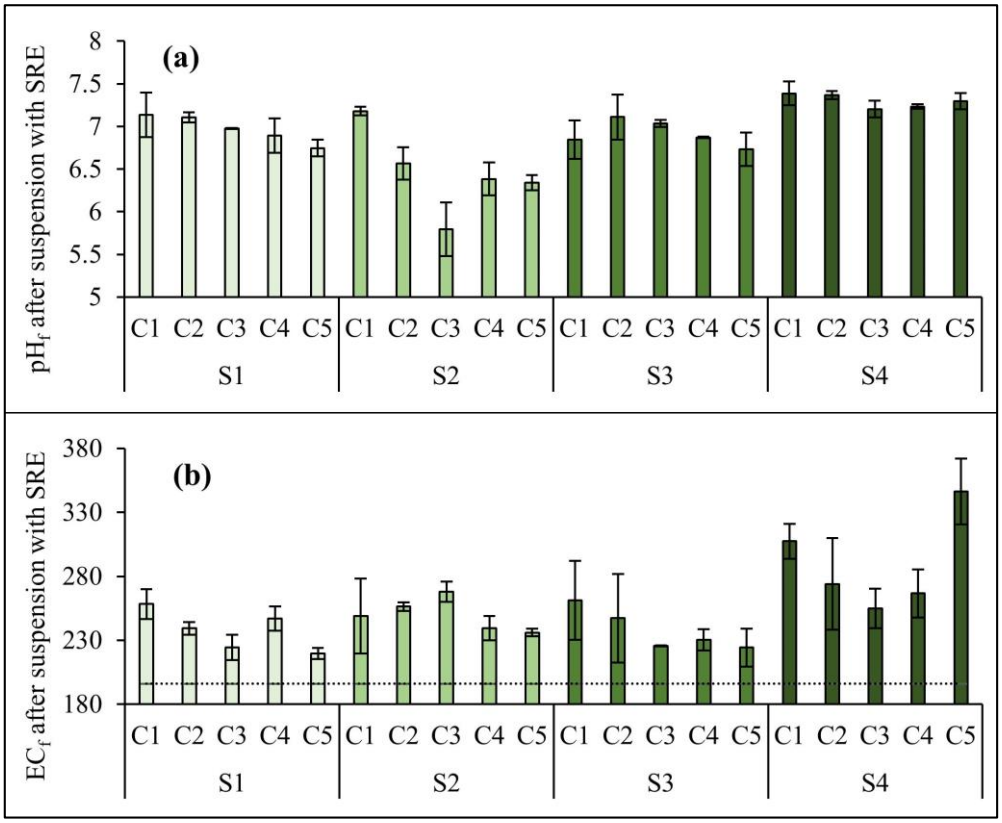

Figure 5: a) pH and b) EC variation after the exposure to SRE. pH_i = 3.37 and EC_i = 196 µS/cm (dotted horizontal line). Whiskers indicate standard deviations of the triplicates.

S1: 0 – 64 µm, S2: 64 – 250 µm, S3: 250 – 500 µm, and S4: 500 – 2000 µm.

3.2.2. Metal behavior after the exposure to synthetic root exudate

As much as 5 mg/g of Cu was released after the addition of SRE (Figure 6a). In terms of percentage (i.e. released Cu out of the sorbed Cu from the Cu sorption experiment), the values were relatively low, notably for samples treated with high Cu concentrations (Figure 6b). As the case of Cu sorption, Cu release was similar for the different fractions after mixing with SRE. The remaining Cu is thought to have formed stable complexes, such as inner monodentate or bidentate sphere complexes to C, N, P, and O functional groups of organic matter (e.g. Moon and Peacock, 2012; Sheals et al., 2001; Strawn and Baker, 2009). In the Cu sorption experiment, the treatments with higher Cu concentrations released higher Ca and Mg concentrations (Figure 3b and c); this indicates that the remaining cations that can be further released by SRE are minimal for those treatments, as generally seen in the C5 treatments (Figure 6c and d). Magnesium release showed a logarithmic decreasing trend for the different sediment fractions. The highest Mg release was recorded for S4, followed by S3, S2, and finally S1. However, S4C5 showed a relatively higher Mg release. Again, this sample had relatively higher EC_f and pH_f values (Figure 5), which suggest that Mg was released among other cations to buffer the pH. Indeed, S4C5 showed a relatively high Ca release (Figure 6c), which further supports the aforesaid notion. Calcium release followed a similar behavior to Mg. However, S4 showed a peculiar behavior, while the other fractions (S1 – S3) were quite similar (Figure 6c). It is worth noting that the logarithmic trend was clear for all the grain sizes concerning Ca and Mg release, except for Ca release in S4 (as indicated by the R^2 values in Figure 6c and d). The average Ca and Mg concentrations released from the control samples (that were treated with 0 mg/L Cu solutions) showed the highest values in comparison to those that were treated with Cu. The values for Ca and Mg release were 56 and 5.0, 57 and 6.1, 54 and 6.9, and 57 and 7.0 mg/L for

239 S1, S2, S3, and S4, respectively (the data are not included in the graphs for clarity reasons). As
240 for the monovalent cations (Na and K), they did not show a clear trend (SM 7).

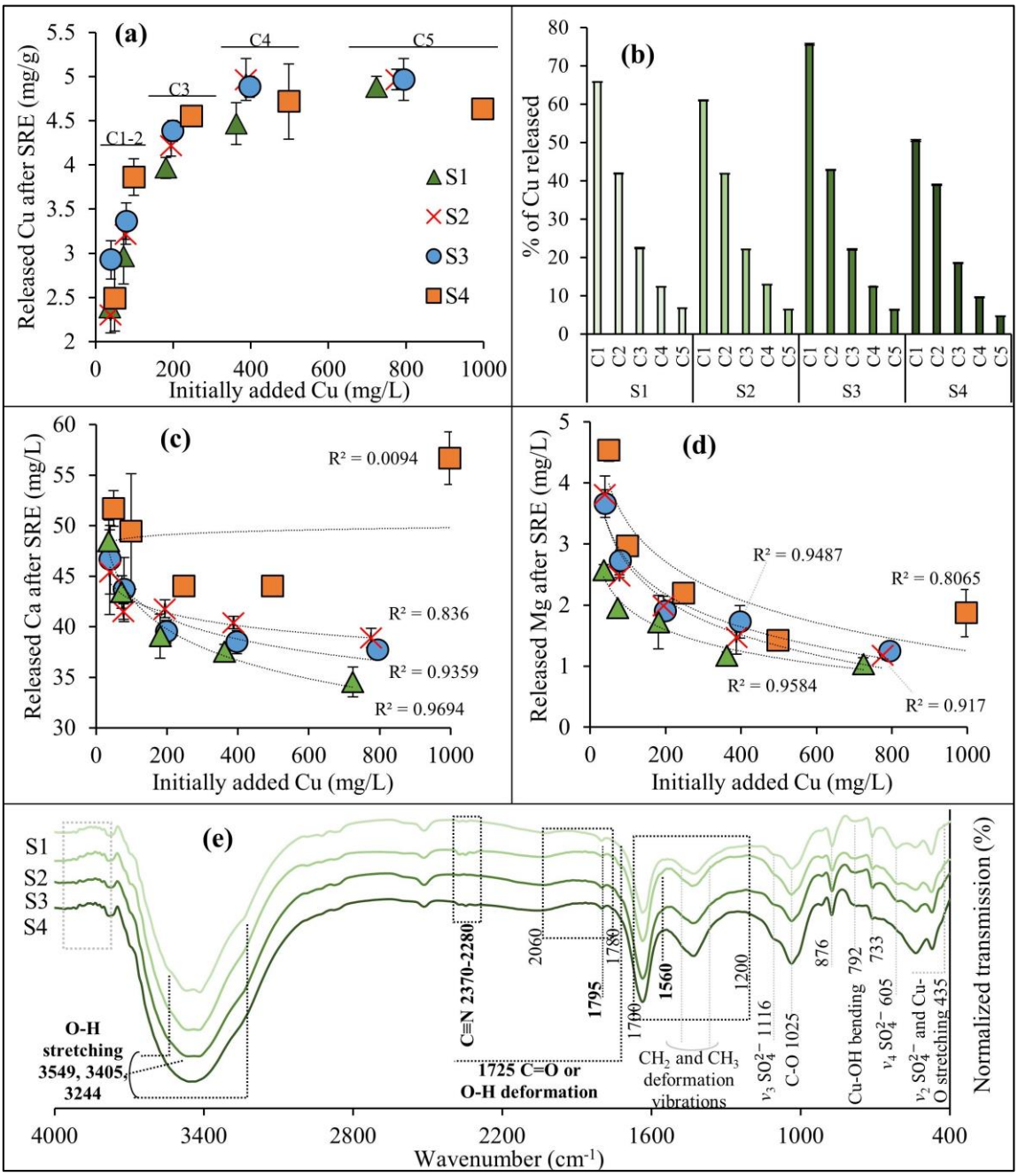

Figure 6: a) The contents of released Cu (mg/g) after the exposure to SRE for the different grain sizes and b) the percentage of Cu released out of the sorbed Cu from the sorption experiment. The concentrations of c) Ca and d) Mg released after the exposure to SRE for the different grain sizes. Whiskers indicate standard deviations of the triplicates. e) FTIR

spectra of the sediment fractions after the exposure to SRE (the example of C1 treatment is given here). The peaks assigned to changes due to Cu sorption are indicated in bold.
S1: 0 – 64 µm, S2: 64 – 250 µm, S3: 250 – 500 µm, and S4: 500 – 2000 µm

3.2.3. The ability of SRE to restore the mineral and chemical status of the sediments

The deformed peak at 1725 cm^{-1}, the small peaks in the 1700 – 1200 cm^{-1} region, and the peak at 1560 cm^{-1} that protruded after Cu sorption disappeared or significantly decreased after mixing with SRE (Figure 6e); the peaks at 3549, 3405, and 3244 cm^{-1} (partially belonging to posnjakite) in S3 almost disappeared after mixing with SRE as well. This strongly suggests that those peaks represent exchangeable binding sites for Cu. Moreover, the peaks at 1795 cm^{-1} (aliphatic or aromatic), the nitrile group at 2370 – 2280 cm^{-1}, and the C-O peak at 1025 cm^{-1} (mainly seen in S1 and S3) disappeared or significantly decreased after Cu sorption (Figure 4b); those peaks reemerged after mixing with SRE (Figure 6e), suggesting that those functional groups are responsible for the exchangeable binding of Cu, such as the formation of Cu-C bonds (e.g. Golubeva et al., 2013; Q. Li et al., 2018). Consequently, this indicates that SRE was able to partially restore the chemical and mineral state of the sediments. The detectable and possibly exchangeable Cu bindings sites belong to organic matter, as reported by other studies (e.g. Eggleton and Thomas, 2004; Kanbar et al., 2018; Q. Li et al., 2018; Matar et al., 2015; Shi et al., 2018). Furthermore, the carbonyl moiety is considered as one of the critical sites for Cu mobility (Moon and Peacock, 2012).

In this study, we focused on the behavior of Cu at the solid-liquid interface in a relatively simple system (Cu dissolved in ultrapure water and an SRE solution); which is a first step towards understanding Cu-sediment interaction in complex ones. Therefore, the results might not be applicable in the case of lake systems. The next step would be to make the experimental conditions resemble lake waters and see the behavior of other metals (e.g. As, Cd, Zn, and Fe) as well. Finally, a summarizing schema representing the main sorption and desorption

processes of Ca, Mg, and Cu onto and from the organic and mineral parts of the sediments is presented (Figure 7).

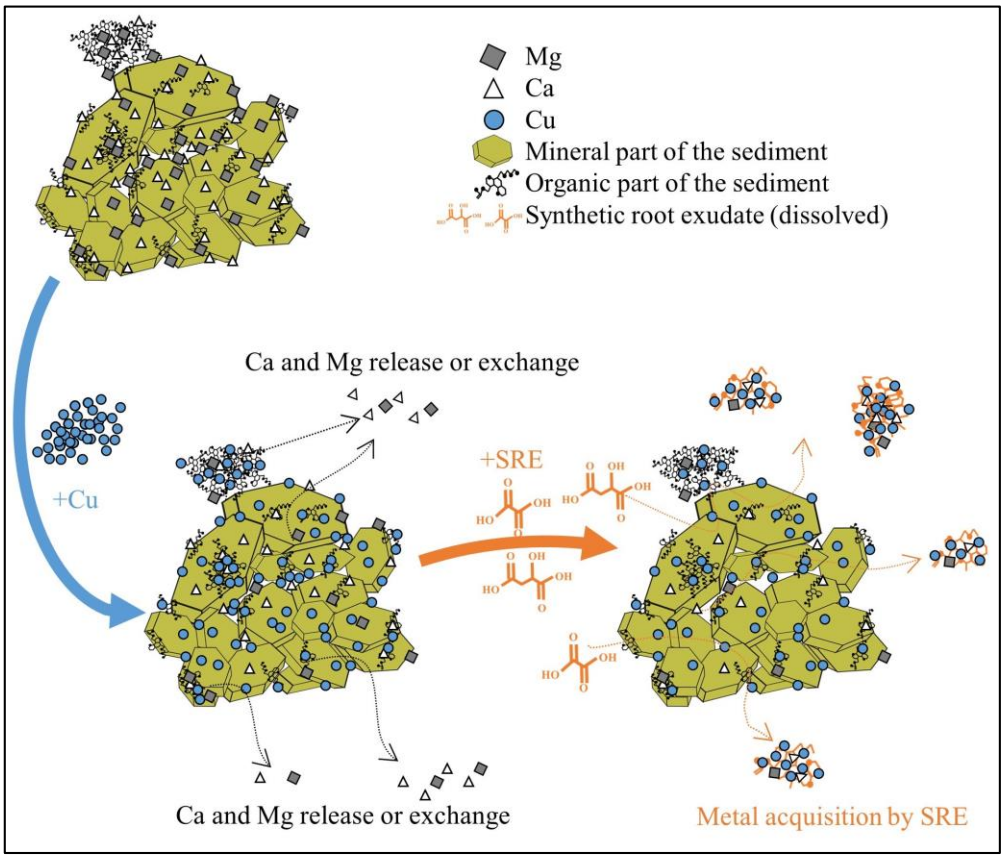

Figure 7: Schematic representation of the main sorption processes of Cu followed by the release of Ca and Mg, and the desorption of Cu, Ca, and Mg after the exposure to synthetic root exudate (SRE). The schema roughly represents the sites where the metals are most likely to be associated (mineral and organic parts); the number of the cations (shapes) is also roughly representative of the data (according to the text). Schema not drawn to scale.

4. Conclusion

Lake sediments were collected from the Qaraaoun reservoir and divided into four fractions (0 – 64 µm, 64 – 250 µm, 250 – 500 µm, and 500 – 2000 µm). The bulk mineralogy and the functional groups were comparable, while the physicochemical parameters and the organic matter and chemical contents were different. The sorption and desorption of copper

were peculiar in the coarsest fraction due to the abundance of organo-mineral complexes. The Cu sorption experiment evidenced that Ca and Mg are the main cations that are exchanged; Ca is mainly released from the surface while Mg is released from the inner structure of the sediment particles and aggregates. Furthermore, Cu sorption mainly occurred on the organic fraction. Interestingly, synthetic root exudate was able to desorb some of the Cu that was bound to exchangeable sites of organic matter. The sorption and desorption of Cu did not vary for the different fractions. However, a variation in the exchanged Ca and Mg concentrations was seen, where the coarsest particles had the highest Ca and Mg release after Cu sorption and after SRE treatment. Finally, and based on the geochemical composition of the matrix, the understanding of Cu-sediment interaction opens the way for safe re-use of Cu-rich media in the environment (e.g. soil amendments).

5. Declaration of Interest

None.

6. Acknowledgment

This research was financed by the research grant programs of the Lebanese University (The funding source had no involvement in the study design, writing of the report, and decision to submit the article for publication). We would like to thank the research assistants of the Research and Analysis Platform for Environmental Sciences (PRASE), namely Ms. Sarah Haddad (zeta potential), Ms. Sahar Rihane and Ms. Malak Tofeily (FTIR), Ms. Manal Houhou-Hadada and Mr. Ali Berro (AAS), and Ms. Layal Hajjar (assistance in laboratory work). We also thank Mr. Nassar Nassar who helped during the sampling campaign, Ms. Delennda Akoum and Ms. Zaynab Nemr for participating in part of the Cu desorption experiment, and two anonymous reviewers for their critical review and constructive comments that improved the quality of this paper.

294

7. References

Acosta, J.A., Martínez-Martínez, S., Faz, A., Arocena, J., 2011. Accumulations of major and trace elements in particle size fractions of soils on eight different parent materials. Geoderma 161, 30–42. https://doi.org/10.1016/j.geoderma.2010.12.001

Al-Qunaibit, M.H., Mekhemer, W.K., Zaghloul, A.A., 2005. The adsorption of Cu(II) ions on bentonite - A kinetic study. J. Colloid Interface Sci. 283, 316–321. https://doi.org/10.1016/j.jcis.2004.09.022

Alcacio, T.E., Hesterberg, D., Chou, J.W., Martin, J.D., Beauchemin, S., Sayers, D.E., 2001. Molecular scale characteristics of Cu(II) bonding in goethite-humate complexes. Geochim. Cosmochim. Acta 65, 1355–1366. https://doi.org/10.1016/S0016-7037(01)00546-4

Ammar, R., Kazpard, V., Wazne, M., El Samrani, A.G., Amacha, N., Saad, Z., Chou, L., 2015. Reservoir sediments: a sink or source of chemicals at the surface water-groundwater interface. Environ. Monit. Assess. 187:579. https://doi.org/10.1007/s10661-015-4791-0

Arias, M., Pérez-Novo, C., López, E., Soto, B., 2006. Competitive adsorption and desorption of copper and zinc in acid soils. Geoderma 133, 151–159. https://doi.org/10.1016/j.geoderma.2005.07.002

Azzi, V., Kazpard, V., Lartiges, B., Kobeissi, A., Kanso, A.A., El Samrani, A.G., 2017. Trace metals in phosphate fertilizers used in eastern Mediterranean countries. Clean - Soil, Air, Water 45, 8. https://doi.org/10.1002/clen.201500988

Badri, D. V., Vivanco, J.M., 2009. Regulation and function of root exudates. Plant, Cell Environ. 32, 666–681. https://doi.org/10.1111/j.1365-3040.2009.01926.x

Carrillo-González, R., Šimůnek, J., Sauvé, S., Adriano, D.C., 2006. Mechanisms and Pathways of Trace Element Mobility in Soils, in: Advances in Agronomy. pp. 111–178.

https://doi.org/10.1016/S0065-2113(06)91003-7

Chen, W., Habibul, N., Liu, X.Y., Sheng, G.P., Yu, H.Q., 2015. FTIR and synchronous fluorescence heterospectral two-dimensional correlation analyses on the binding characteristics of copper onto dissolved organic matter. Environ. Sci. Technol. 49, 2052–2058. https://doi.org/10.1021/es5049495

Du Laing, G., Rinklebe, J., Vandecasteele, B., Meers, E., Tack, F.M.G., 2009. Trace metal behaviour in estuarine and riverine floodplain soils and sediments: A review. Sci. Total Environ. 407, 3972–3985. https://doi.org/10.1016/j.scitotenv.2008.07.025

Du Laing, G., Vandecasteele, B., De Grauwe, P., Moors, W., Lesage, E., Meers, E., Tack, F.M.G., Verloo, M.G., Grauwe, P. De, 2007. Factors affecting metal concentrations in the upper sediment layer of intertidal reedbeds along the river Scheldt. J. Environ. Monit. 9, 449–455. https://doi.org/10.1039/b618772b

Eggleton, J., Thomas, K. V., 2004. A review of factors affecting the release and bioavailability of contaminants during sediment disturbance events. Environ. Int. 30, 973–980. https://doi.org/10.1016/j.envint.2004.03.001

Fariña, A.O., Peacock, C.L., Fiol, S., Antelo, J., Carvin, B., 2018. A universal adsorption behaviour for Cu uptake by iron (hydr)oxide organo-mineral composites. Chem. Geol. 479, 22–35. https://doi.org/10.1016/j.chemgeo.2017.12.022

Gallé, T., Van Lagen, B., Kurtenbach, A., Bierl, R., 2004. An FTIR-DRIFT study on river sediment particle structure: Implications for biofilm dynamics and pollutant binding. Environ. Sci. Technol. 38, 4496–4502. https://doi.org/10.1021/es040005m

Golubeva, E.N., Zubanova, E.M., Zhidomirov, G.M., 2013. The nature of Cu-C bond and copper oxidation state in chloroorganocuprates [CuClnCH3]2-n. J. Phys. Org. Chem. 26,

724–729. https://doi.org/10.1002/poc.3093

Grabowski, R.C., Droppo, I.G., Wharton, G., 2011. Erodibility of cohesive sediment: The importance of sediment properties. Earth-Science Rev. 105, 101–120. https://doi.org/10.1016/j.earscirev.2011.01.008

Grayston, S.J., Vaughan, D., Jones, D., 1997. Rhizosphere carbon flow in trees, in comparison with annual plants: The importance of root exudation and its impact on microbial activity and nutrient availability. Appl. Soil Ecol. 5, 29–56. https://doi.org/10.1016/S0929-1393(96)00126-6

Hossain, M.A., Piyatida, P., da Silva, J.A.T., Fujita, M., 2012. Molecular mechanism of heavy metal toxicity and tolerance in plants: Central role of glutathione in detoxification of reactive oxygen species and methylglyoxal and in heavy metal chelation. J. Bot. 2012, 1–37. https://doi.org/10.1155/2012/872875

Huang, Y., Zhao, L., Keller, A.A., 2017. Interactions, transformations, and bioavailability of nano-copper exposed to root exudates. Environ. Sci. Technol. 51, 9774–9783. https://doi.org/10.1021/acs.est.7b02523

Jain, C.K., Sharma, M.K., 2002. Adsorption of cadmium on bed sediments of river Hindon: adsorption models and kinetics. Water. Air. Soil Pollut. 137, 1–19. https://doi.org/10.1023/A:1015530702297

Ju, W., Liu, L., Fang, L., Cui, Y., Duan, C., Wu, H., 2019. Impact of co-inoculation with plant-growth-promoting rhizobacteria and rhizobium on the biochemical responses of alfalfa-soil system in copper contaminated soil. Ecotoxicol. Environ. Saf. 167, 218–226. https://doi.org/10.1016/j.ecoenv.2018.10.016

Kanbar, H.J., Hanna, N., El Samrani, A.G., Kobaissi, A.N., Harb, N., Kazpard, V., Amacha,

N., 2014. Metal binding in soil cores and sediments in the vicinity of a dammed agricultural and industrial watershed. Environ. Monit. Assess. 186, 8793–8806. https://doi.org/10.1007/s10661-014-4044-7

Kanbar, H.J., Srouji, E.E., Zeidan, Z., Chokr, S., Matar, Z., 2018. Leaching of metals in coastal technosols triggered by saline solutions and labile organic matter removal. Water, Air, Soil Pollut. 229, 157. https://doi.org/10.1007/s11270-018-3808-z

Kobaissi, A.N., Kanso, A.A., Kanbar, H.J., 2014. Translocation of heavy metals in Zea mays L. treated with wastewater and consequences on morphophysiological aspects. Rev. Int. Contam. Ambient. 30, 297–305.

Lee, Y., Choi, J., Lee, K.J., Stott, N.E., Kim, D., 2008. Large-scale synthesis of copper nanoparticles by chemically controlled reduction for applications of inkjet-printed electronics. Nanotechnology 19, 415604. https://doi.org/10.1088/0957-4484/19/41/415604

Li, K., Wang, P., Qian, J., Wang, C., Xing, L., Liu, J., Tian, X., Lu, B., Tang, W., 2018. Effects of sediment components and TiO2 nanoparticles on perfluorooctane sulfonate adsorption properties. J. Soils Sediments. https://doi.org/10.1007/s11368-018-2115-z

Li, Q., Du, H., Chen, W., Hao, J., Huang, Q., Cai, P., Feng, X., 2018. Aging shapes the distribution of copper in soil aggregate size fractions. Environ. Pollut. 233, 569–576. https://doi.org/10.1016/j.envpol.2017.10.091

Liu, P.Y., Wen, Q.L., Li, Y.J., Dong, C.X., Pan, G.X., 2015. Kinetics of specific and non-specific copper sorption on aggregates of an acidic paddy soil from the Taihu Lake region in East China. Pedosphere 25, 37–45. https://doi.org/10.1016/S1002-0160(14)60074-6

Matar, Z., Soares Pereira, C., Chebbo, G., Uher, E., Troupel, M., Boudahmane, L., Saad, M.,

Gourlay-France, C., Rocher, V., Varrault, G., 2015. Influence of effluent organic matter on copper speciation and bioavailability in rivers under strong urban pressure. Environ. Sci. Pollut. Res. 22, 19461–19472. https://doi.org/10.1007/s11356-015-5110-6

Moon, E.M., Peacock, C.L., 2012. Adsorption of Cu(II) to ferrihydrite and ferrihydrite-bacteria composites: Importance of the carboxyl group for Cu mobility in natural environments. Geochim. Cosmochim. Acta 92, 203–219. https://doi.org/10.1016/j.gca.2012.06.012

Ratasuk, P., Parkpian, P., Jugsujinda, A., DeLaune, R.D., 2003. Factors governing adsorption and distribution of Copper in Samut Prakarn coastal sediment, Thailand. J. Environ. Sci. Heal. Part A 38, 1793–1810. https://doi.org/10.1081/ESE-120022879

Seniunaite, J., Vasarevicius, S., 2017. Leaching of copper, lead and zinc from municipal solid waste incineration bottom ash. Energy Procedia 113, 442–449. https://doi.org/10.1016/j.egypro.2017.04.036

Sheals, J., Persson, P., Hedman, B., 2001. IR and EXAFS spectroscopic studies of glyphosate protonation and copper(II) complexes of glyphosate in aqueous solution. Inorg. Chem. 40, 4302–4309. https://doi.org/10.1021/ic000849g

Shi, H., Li, Q., Chen, W., Cai, P., Huang, Q., 2018. Distribution and mobility of exogenous copper as influenced by aging and components interactions in three Chinese soils. Environ. Sci. Pollut. Res. 25, 10771–10781. https://doi.org/10.1007/s11356-018-1288-8

Strawn, D.G., Baker, L.L., 2009. Molecular characterization of copper in soils using X-ray absorption spectroscopy. Environ. Pollut. 157, 2813–2821. https://doi.org/10.1016/j.envpol.2009.04.018

Veli, S., Alyüz, B., 2007. Adsorption of copper and zinc from aqueous solutions by using natural clay. J. Hazard. Mater. 149, 226–233.

https://doi.org/10.1016/j.jhazmat.2007.04.109

Yamasaki, H., Pilon, M., Shikanai, T., 2008. How do plants respond to copper deficiency? Plant Signal. Behav. 3, 231–232. https://doi.org/10.4161/psb.3.4.5094

Yuan, G.D., Theng, B.K.G., Churchman, G.J., Gates, W.P., 2013. Clays and Clay Minerals for Pollution Control, in: Bergaya, F., Lagaly, G. (Eds.), Handbook of Clay Science. Part B: Techniques and Applications. Elsevier, pp. 587–644. https://doi.org/10.1016/B978-0-08-098259-5.00021-4

Zaffino, C., Guglielmi, V., Faraone, S., Vinaccia, A., Bruni, S., 2015. Exploiting external reflection FTIR spectroscopy for the in-situ identification of pigments and binders in illuminated manuscripts. Brochantite and posnjakite as a case study. Spectrochim. Acta - Part A Mol. Biomol. Spectrosc. 136, 1076–1085. https://doi.org/10.1016/j.saa.2014.09.132

Zittlau, A.H., Shi, Q., Boerio-Goates, J., Woodfield, B.F., Majzlan, J., 2013. Thermodynamics of the basic copper sulfates antlerite, posnjakite, and brochantite. Chemie der Erde 73, 39–50. https://doi.org/10.1016/j.chemer.2012.12.002

8. Supplementary Materials

Mineral and chemical changes of sediments after Cu sorption and then desorption induced by synthetic root exudate

Hussein Jaafar Kanbar [a, b, c *] and Malak Kaouk[a]

[a] Applied Plant Biotechnology Laboratory (APBL). Faculty of Sciences, Department of Earth and Life Sciences. The Lebanese University, Rafic Hariri Campus, Hadat, Lebanon.

[b] Research and Analysis Platform for Environmental Sciences (PRASE), Doctoral School of Sciences and Technology (EDST). Faculty of Sciences. The Lebanese University, P.O. 5, Rafic Hariri Campus, Hadat, Lebanon.

[c] Department of Chemistry, Umeå University, SE-901 87, Umeå, Sweden.

* Corresponding author: Hsen.kanbar@gmail.com

ORCID ID: 0000-0002-9505-9974

SM 1: Sedimentary materials: mineralogical, physicochemical, and chemical parameters

Methodology

Mineralogical composition

The major and well crystalline minerals were detected by qualitative X-ray diffraction (XRD) using a D8 Bruker X-ray diffractometer (Cu K_α source of wavelength 1.5418 Å). The diffractograms were collected in the 2θ range between 3° and 64°, and with a step size of 0.034° and a 3 sec collecting time. The functional groups were detected by Fourier transform infrared (FTIR-6300 from JASCO). The spectra were collected from 4000 to 400 cm^{-1}.

Physicochemical characterization

Each sediment fraction was analyzed for physicochemical parameters, namely cation exchange capacity (CEC), pH, electric conductivity (EC), salinity, total dissolved solids (TDS), and zeta potential. All the samples were run as duplicates except CEC, which was run as triplicates. The CEC was determined by replacing the exchangeable cations of each fraction by copper (Thien and Graveel, 2003). As for pH measurements, a 1:5 volumetric ratio of sediment:KCl (1M) was stirred for an hour, let to settle, and the pH was measured using a combined soil pH electrode (MA920B/1 from Milwaukee). The EC, salinity, and TDS were measured by creating a 1:5 volumetric ratio of sediment:distilled water, according to AFNOR (NF ISO 11265, 1994); after vigorously stirring for one hour and resting for 30 minutes, the EC, TDS, and salinity values were measured using a LaMotte pH/TDS/Salt portable meter (Tracer PockeTester). The organic matter content was estimated by loss on ignition (LoI) after calcinating the fractions at 550°C for four hours (Heiri et al., 2001). The surface charge or zeta potential (ζ-potential in mV) of each sediment fraction was determined by Zeta Meter 4.0 (Zeta-Meter, Inc, USA).

Metal content

The chemical composition of the sediment fractions was determined after digestion with aqua regia (each sample was run as triplicates). Briefly, 1 g of finely ground sediment fraction was digested with a 1:3 (v:v) solution of HNO_3:HCl (more information is found in Kanbar et al., (2014)). The metals (Cu, Pb, Cr, Mn, Fe, Zn, Mg, Cd, and Ca) were quantified by atomic absorption spectroscopy (AAS Rayleigh WFX-210) equipped with a WF-10A autosampler and flame and graphite furnace modes; the concentrations of Na and K were determined by flame photometry (AFP100 flame photometer, from Biotech Engineering Management Co. Ltd.).

Manually prepared standards were used for calibration and QA/QC procedures were implemented based on external standards. Reproducibility and accuracy of the measurements were validated by external calibrations that were run between every ~10 samples. The values were taken unless the error exceeded 5-10%. The quantification and detection limits (LOQ and LOD, respectively) were calculated according to the ICH Harmonised Tripartite Guideline (ICH Harmonized Tripartite Guideline, 2005). The LOD was calculated as 3.3 times the standard deviation (σ) of the response of reference materials over the slope (s) of the calibration curve (over 25 measurements). The LOQ was calculated as 10 times the standard deviation (σ) of the response of reference materials over the slope (s) of the calibration curve (over 25 measurements).

Results

Mineralogical composition (XRD and FTIR)

The mineralogical composition of the sediment fractions was quite similar, except for the detection of feldspar in S1 (see figure below). The well crystalline minerals in the sediment fractions are calcite (carbonate mineral), quartz (primary silicate mineral), and phyllosilicates (secondary weathered silicate minerals) such as kaolinite. The presence of calcite in the sediments is anticipated due to the carbonaceous geological formation, high Ca contents, and alkaline pH (see figure below) (Abdel-Rahman and Nader, 2002; Ammar et al., 2015; Kanbar et al., 2014). Phyllosilicates, as indicated by the diffraction lines at 7.14, 4.47, and 2.57 Å were also detected in S4. Even though phyllosilicates are fine materials (clays), their presence in the coarsest fraction (S4) indicates that these coarse particles certainly contain aggregates, such as organo-mineral complexes.

Similar to XRD, the FTIR results showed comparable findings among the different fractions (see figure below). The bands at 520 and 465 cm^{-1} might indicate salt (Parikh et al., 2014). The presence of the 620 cm^{-1} band could indicate Fe-O vibrations of Fe oxyhydroxides; indeed, that peak was prominent in S4, which also had the highest Fe content. The samples also showed aromatic C-H (915, 875, 785, and 710 cm^{-1}), C-O groups of carboxylic acid (1115 and 1025 cm^{-1}), aliphatic or aromatic compounds (1800 – 1400 cm^{-1}), nitrile C≡N groups (2370 – 2280 cm^{-1}), alkyl functional groups (-CH3, -CH2, and CH between 2960 and 2855 cm^{-1}), C=C groups of aromatic alkenes (1640 cm^{-1}), and O-H groups of carboxylic acid (3435, 3351, and 3300, and 2515 cm^{-1}), indicating organic matter (Bishop et al., 2013; Levard et al., 2012; Margenot et al., 2015; Parikh et al., 2014; Schuttlefield et al., 2007). Moreover, the bands

503 between 930 – 730 cm^{-1} and 1425 cm^{-1} could also indicate calcite (Legodi et al., 2001), which
504 was predominantly detected by XRD; bands at 1115 and 1025 cm^{-1} can also indicate Si-O-Si
505 quartz bond and Si-O stretching of silicates/clays, and the 2515 cm^{-1} peak could refer to thiol
506 (S-H) (Bishop et al., 2013; Parikh et al., 2014). Moreover, the peak at 1640 cm^{-1} might indicate
507 the bending mode of water molecules, C=O from amides, and carboxylates (Parikh et al., 2014).
508 In addition, kaolinite was slightly detected by XRD (7.14Å), which is supported by the
509 vibration bands between 3800 and 3500 cm^{-1} and belong to the O-H stretching motion of
510 interlayer hydroxyl groups of kaolinite (Schuttlefield et al., 2007).

511 Initial physicochemical parameters

512 The different sediment fractions showed alkaline pH (7.5 – 8), with higher alkalinity for
513 finer particles. These alkaline pH values reflect the calcareous nature of the geological
514 formation of the Litani watershed (Abdel-Rahman and Nader, 2002). The CEC and LoI values
515 ranged between 22 and 31 meq/100g and between 6.0% and 8.7%, respectively (part a of the
516 figure below). Those findings are similar to other studies conducted in the vicinity of the
517 Qaraaoun reservoir (Ammar et al., 2016, 2015; Kanbar et al., 2014; Wazne and Korfali, 2016).
518 In general, elevated CEC in sediments is due to organic matter and certain clay minerals
519 (e.g. Manceau et al., 2002). Interestingly, the coarsest fraction S4 (500 – 2000 µm) had the
520 highest organic content and CEC. This suggests that the elevated CEC values are due to organic
521 matter, rather than fine mineral particles (i.e. clays). Another possibility would be the presence
522 of organo-mineral complexes that explain high CEC and OM in the coarse fraction. The EC,
523 TDS, and salinity values were also different among the fractions.

524 Metal contents in the different sediment fractions

525 The coarsest fraction of the sediments was enriched with Cu, Pb, Cr, Mn, Fe, and Zn
526 (part b of the figure below), which is contradictory to the general case (e.g. Du Laing et al.,
527 2007; Prasad et al., 2006; Quenea et al., 2009). In another study in the Qaraaoun reservoir, the
528 metal contents of the sediments did not correlate to particle size (Kanbar et al., 2014). Then
529 again, metals are usually associated to sediments with high OM, which is S4 in our case; the
530 higher metal and organic matter contents are explained by the predominance of organo-mineral
531 complexes in the coarsest fraction. Copper has high affinity to organic matter and Fe
532 oxyhydroxides in riverine and lacustrine systems (e.g. Eggleton and Thomas, 2004; Korfali et
533 al., 2006; Matar et al., 2015; Shi et al., 2018). Potassium and Na showed comparable values
534 between the different fractions, and Ca and Cd were mostly enriched in S1, followed by S2,

S3, and S4 (Figure 1b). The elevated Ca contents are expected due to natural weathering in the watershed. Indeed, the basin is mostly made from carbonaceous materials (Abdel-Rahman and Nader, 2002). It should be noted that the grain sizes in this study represent the actual sizes of the aggregates (i.e. *in situ* sizes); in other words, the aggregates and complexes were not broken during size separation (wet sieving) to maintain the representativeness of the actual lake sediment sizes.

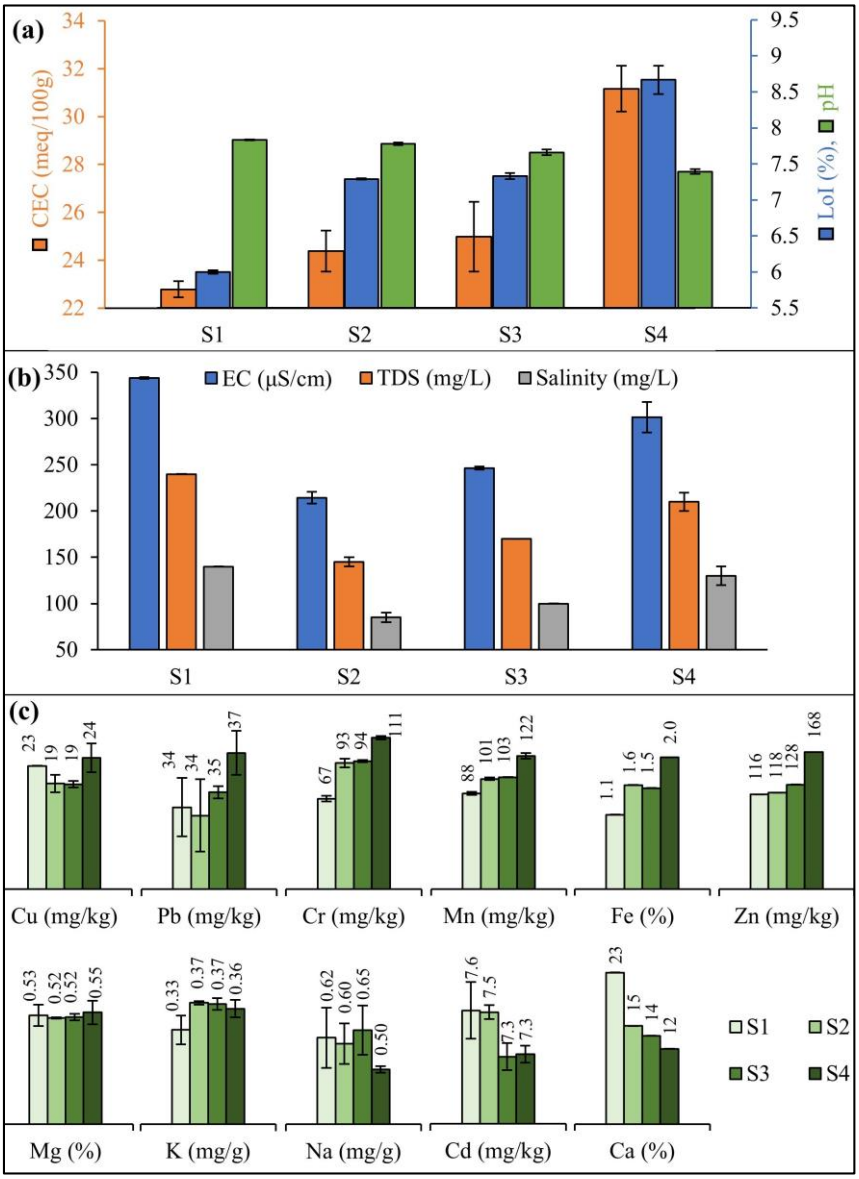

a) CEC (meq/100g), pH, and LoI (%), b) EC (µS/cm), TDS (mg/L), and salinity (mg/L), and c) metal contents (Cu, Pb, Cr, Mn, Zn, and Cd in mg/kg, Fe, Mg, and Ca in %, and K and Na in mg/g) of the different sediment fractions. Whiskers, whenever present, indicate standard deviations of the technical replicates.

S1: 0 – 64 µm, S2: 64 – 250 µm, S3: 250 – 500 µm, and S4: 500 – 2000 µm.

SM 2: The concentrations of Cu (in mg/L and mM) used in the Cu sorption experiment for each fraction and for all the treatments. The Cu concentrations are based on the CEC values. For example, a solution with 0.5CEC equivalent contains a Cu concentration that can fill half of the exchangeable sites for the certain sediment fraction. The average CEC values are included with their standard deviations (n=3).

Fraction	CEC (meq/100g)	Treatment	Equivalent to	Cu (mg/L)	Cu (mM)
S1 0 – 64 µm	22.8±0.3	C1	0.5CEC	36.2	0.57
		C2	1CEC	72.4	1.14
		C3	2.5CEC	181.1	2.85
		C4	5CEC	362.1	5.70
		C5	10CEC	724.3	11.40
S2 64 – 250 µm	24.4±0.8	C1	0.5CEC	39.0	0.61
		C2	1CEC	77.9	1.23
		C3	2.5CEC	194.8	3.07
		C4	5CEC	389.6	6.13
		C5	10CEC	779.1	12.26
S3 250 – 500 µm	25.0±1.4	C1	0.5CEC	39.8	0.63
		C2	1CEC	79.5	1.25
		C3	2.5CEC	198.8	3.13
		C4	5CEC	397.6	6.26
		C5	10CEC	795.3	12.51
S4 500 – 2000 µm	31.2±0.9	C1	0.5CEC	49.5	0.78
		C2	1CEC	99.1	1.56
		C3	2.5CEC	247.7	3.90
		C4	5CEC	495.4	7.80
		C5	10CEC	990.8	15.59

542

543

SM 3: The composition of the synthetic root exudate and the concentrations of the components used in the desorption experiment

Component	Compound	Concentration (mM)
Sugars	Glucose	25
	D-Fructose	25
	Sucrose	25
Small organic acids	Citric acid	12.5
	Malic acid	12.5
	Succinic acid	12.5
	Oxalic acid	12.5
Amino acids	Leucine	6.25
	Proline	6.25

544

SM 4: The pH values before (pH_i) and after (pH_f) the Cu sorption experiment.

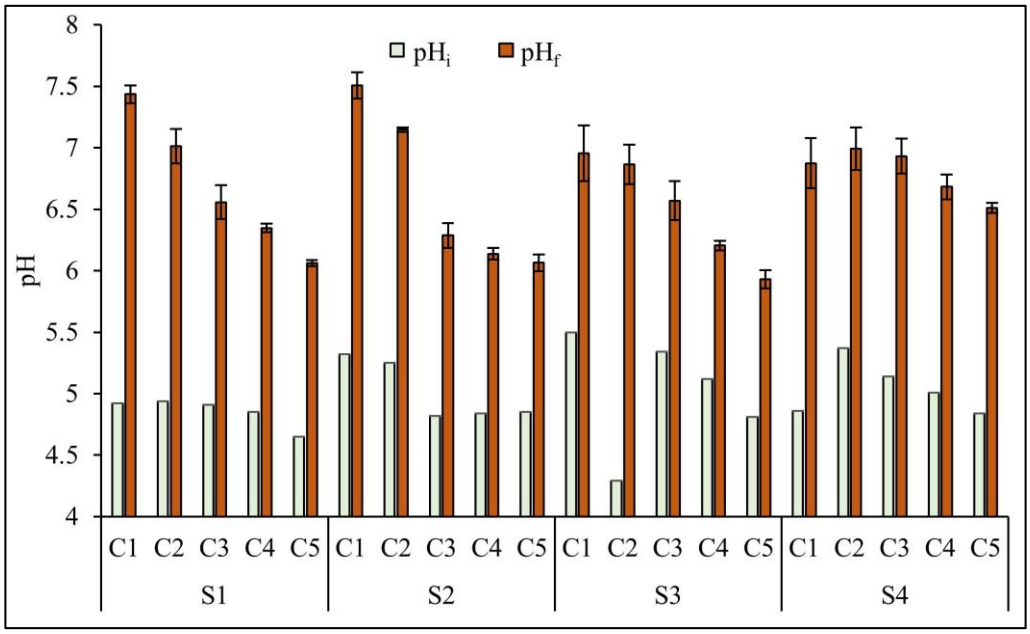

Whiskers indicate standard deviations of the triplicates.

S1: 0 – 64 µm, S2: 64 – 250 µm, S3: 250 – 500 µm, and S4: 500 – 2000 µm

548 SM 5: The percentage of Cu sorbed onto the different sediment fractions after 24 hours.

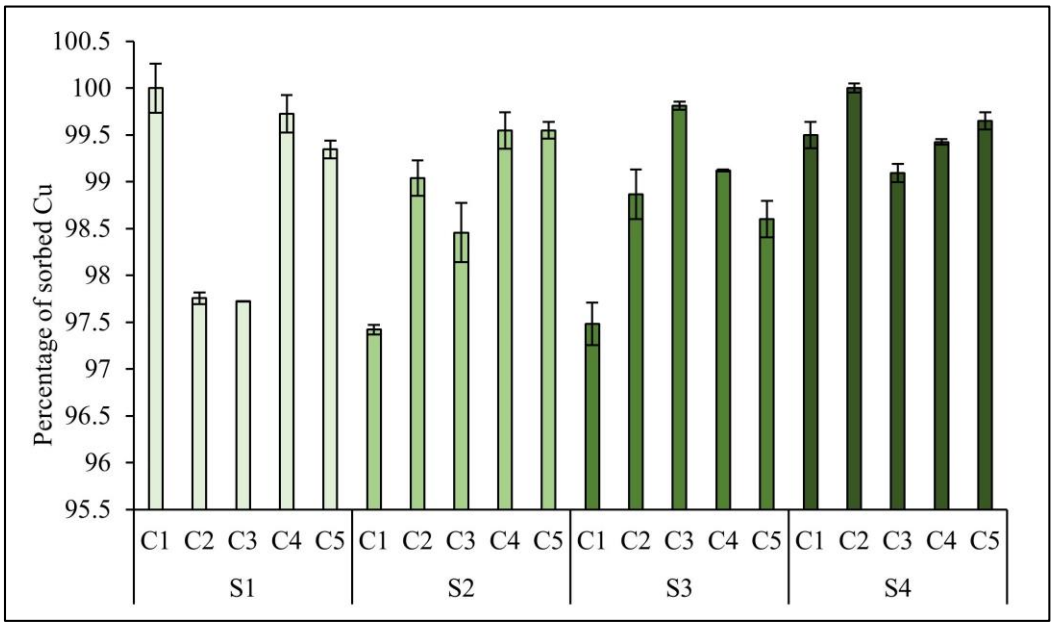

549

550 Whiskers indicate standard deviations of the triplicates.

551 S1: 0 – 64 µm, S2: 64 – 250 µm, S3: 250 – 500 µm, and S4: 500 – 2000 µm

552

SM 6: The concentrations (mg/L) and equivalent contents (mg/g) of Cu in the positive controls.

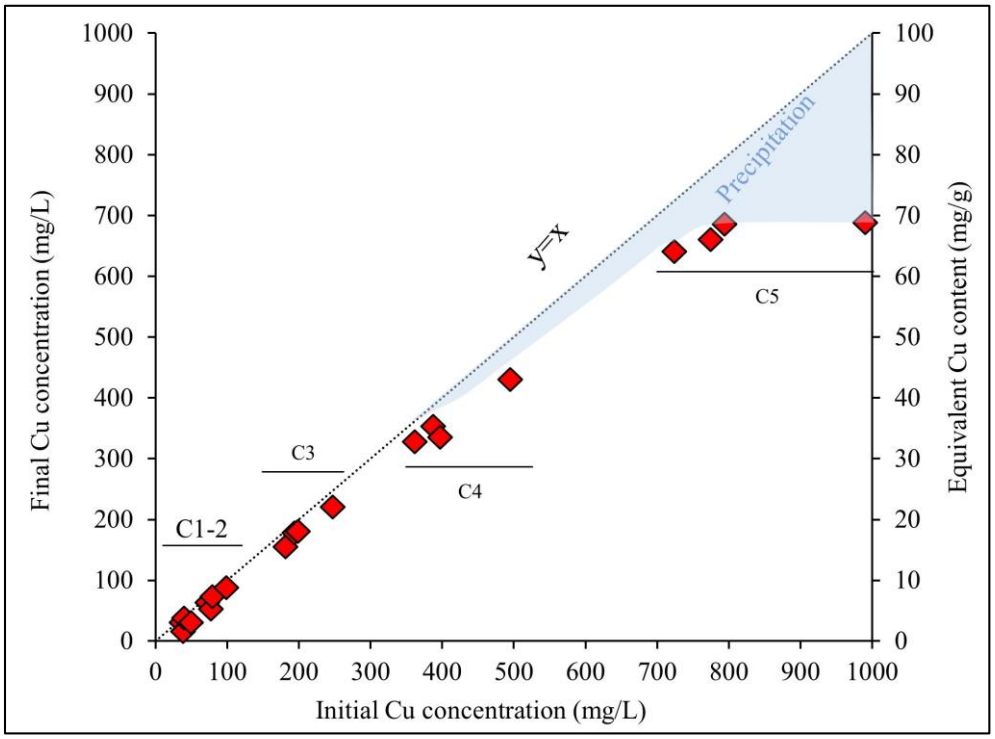

Some of the final Cu concentrations (after 24 hours shaking) were below the initial concentrations in the positive control samples. This indicates that either Cu precipitated or sorbed onto the walls of the tubes during the sorption experiment. Since the final Cu concentrations that shifted below the expected values (y=x in the figure) concerned Cu values above ~ 350 mg/L (i.e. for C4 and C5), the decline in Cu concentration is expected to be due to precipitation (as clearly evidenced in Figure 4a). According to the values given by the positive controls, the qe might be overestimated up to 30% for C5. More specifically, only 688 mg/L of Cu is thought to be sorbed in the case of S4C5, while the rest (300 mg/L) probably precipitated. Therefore, the Cu equilibrium uptake for the treatments with high Cu concentrations might have a margin of error (as indicated by the blue region in Figure 3a).

SM 7: The release of Na and K for different grain sizes and different treatments after Cu sorption (a and b) and after the exposure to SRE (c and d).

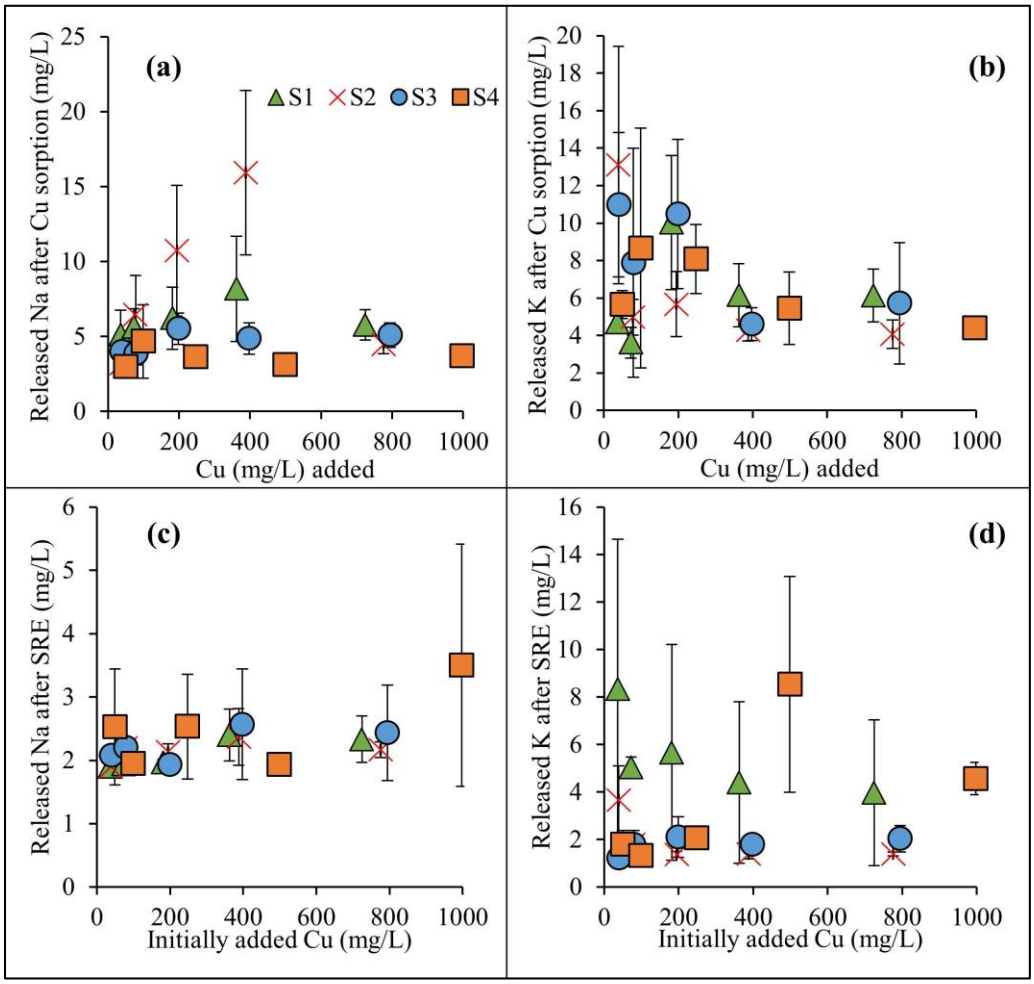

Whiskers indicate standard deviations of the triplicates.

S1: 0 – 64 µm, S2: 64 – 250 µm, S3: 250 – 500 µm, and S4: 500 – 2000 µm

SM 8: Surface charge of the sedimentary materials after Cu sorption.

The negative surface charges of particles, including clays, become less negative upon the sorption of cations (Cu in our case). As expected, the surface charge leaned towards zero as the Cu concentrations in the solutions increased (see figure below). The preference of Cu binding onto surface layers is seen by the critical drop in the surface charges between C0 and C1. Upon further increase in Cu concentrations, the drop in the surface charge was only minor, indicating that Cu binding occurred on sites other than the surface (e.g. exchanged with embedded Mg, as explained in section 3.1.2 in the main text). Interestingly, the surface charge of only S4 reached zero when treated with maximum concentration of Cu (i.e. C5), indicating that no more Cu could sorb onto the surface. This, however, does not mean that Cu cannot further bind to sites other than the surface. This clearly shows that Cu-cation exchange (mainly Ca and Mg) did not solely happen on the surface. Moreover, another notion that should not be overlooked is that the decrease in surface charge reduces the repulsion between particles. Consequently, aggregation occurs, which could also be responsible for further reduction of the zeta potential.

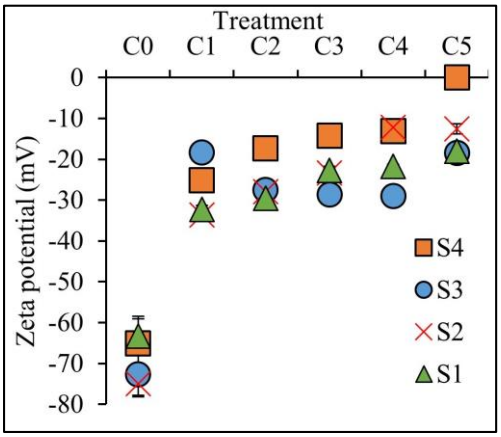

The surface charge of the sediment fractions after Cu sorption for the different treatments. C0: control. S1: 0 – 64 µm, S2: 64 – 250 µm, S3: 250 – 500 µm, and S4: 500 – 2000 µm.

588 SM 9: XRD patterns of S3 after the application of synthetic root exudate

589 At the XRD level, there were no detectable changes in the diffractograms between the samples
590 after Cu sorption and those after the addition of SRE.

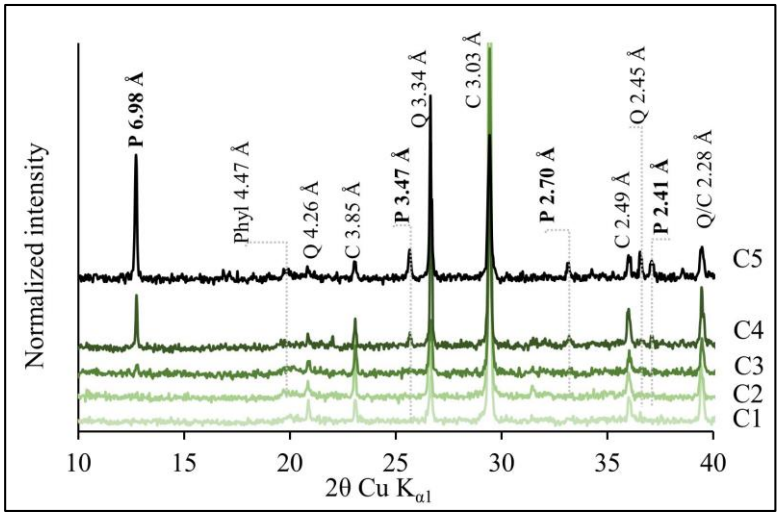

P: posnjakite, Phyl: phyllosilicates, Q: quartz, and C: calcite. The interplanar distances (in Å) and the minerals are assigned to the peaks.

591

592

References

Abdel-Rahman, A.-F.M., Nader, F.H., 2002. Characterization of the Lebanese Jurassic-Cretaceous carbonate stratigraphic sequence: a geochemical approach. Geol. J. 37, 69–91. https://doi.org/10.1002/gj.902

Ammar, R., Kanbar, H.J., Kazpard, V., Wazne, M., El Samrani, A.G., Amacha, N., Saad, Z., Chou, L., 2016. Role of phosphogypsum and NPK amendments on the retention or leaching of metals in different soils. J. Environ. Manage. 178, 20–29. https://doi.org/10.1016/j.jenvman.2016.04.042

Ammar, R., Kazpard, V., Wazne, M., El Samrani, A.G., Amacha, N., Saad, Z., Chou, L., 2015. Reservoir sediments: a sink or source of chemicals at the surface water-groundwater interface. Environ. Monit. Assess. 187:579. https://doi.org/10.1007/s10661-015-4791-0

Bishop, J.L., Ethbrampe, E.B., Bish, D.L., Abidin, Z.L., Baker, L.L., Matsue, N., Henmi, T., 2013. Spectral and hydration properties of allophane and imogolite. Clays Clay Miner. 61, 57–74. https://doi.org/10.1346/CCMN.2013.0610105

Du Laing, G., Vandecasteele, B., De Grauwe, P., Moors, W., Lesage, E., Meers, E., Tack, F.M.G., Verloo, M.G., Grauwe, P. De, 2007. Factors affecting metal concentrations in the upper sediment layer of intertidal reedbeds along the river Scheldt. J. Environ. Monit. 9, 449–455. https://doi.org/10.1039/b618772b

Eggleton, J., Thomas, K. V., 2004. A review of factors affecting the release and bioavailability of contaminants during sediment disturbance events. Environ. Int. 30, 973–980. https://doi.org/10.1016/j.envint.2004.03.001

Heiri, O., Lotter, A.F., Lemcke, G., 2001. Loss on ignition as a method for estimating organic and carbonate content in sediments: reproducibility and comparability of results. J. Paleolimnol. 25, 101–110. https://doi.org/10.1023/A:1008119611481

ICH Harmonized Tripartite Guideline, 2005. Validation of analytical procedures: text and methodology Q2 (R1), in: International Conference on Harmonization of Technical Requirements for Registration of Pharmaceuticals for Human Use. Geneva, Switzerland, p. 13.

Kanbar, H.J., Hanna, N., El Samrani, A.G., Kobaissi, A.N., Harb, N., Kazpard, V., Amacha, N., 2014. Metal binding in soil cores and sediments in the vicinity of a dammed agricultural

622 and industrial watershed. Environ. Monit. Assess. 186, 8793–8806.
623 https://doi.org/10.1007/s10661-014-4044-7

624 Korfali, S.I., Jurdi, M., Davies, B.E., 2006. Variation of metals in bed sediments of Qaraaoun
625 Reservoir, Lebanon. Environ. Monit. Assess. 115, 307–319. https://doi.org/10.1007/s10661-
626 006-6556-2

627 Legodi, M.A., De Waal, D., Potgieter, J.H., Potgieter, S.S., 2001. Rapid determination of
628 CaCO3 in mixtures utilising FT-IR spectroscopy. Miner. Eng. 14, 1107–1111.
629 https://doi.org/10.1016/S0892-6875(01)00116-9

630 Levard, C., Doelsch, E., Basile-Doelsch, I., Abidin, Z., Miche, H., Masion, A., Rose, J.,
631 Borschneck, D., Bottero, J.-Y., 2012. Structure and distribution of allophanes, imogolite and
632 proto-imogolite in volcanic soils. Geoderma 183–184, 100–108.
633 https://doi.org/10.1016/j.geoderma.2012.03.015

634 Manceau, A., Marcus, M.A., Tamura, N., 2002. Quantitative speciation of heavy metals in soils
635 and sediments by synchrotron X-ray techniques. Rev. Mineral. Geochemistry 49, 341–428.
636 https://doi.org/10.2138/gsrmg.49.1.341

637 Margenot, A., Calderón, F., Bowles, T., Parikh, S., Jackson, L., 2015. Soil organic matter
638 functional group composition in relation to organic carbon, nitrogen, and phosphorus practions
639 in organically managed tomato fields. Soil Sci. Soc. Am. J. 79, 772–782.
640 https://doi.org/10.2136/sssaj2015.02.0070

641 Matar, Z., Soares Pereira, C., Chebbo, G., Uher, E., Troupel, M., Boudahmane, L., Saad, M.,
642 Gourlay-France, C., Rocher, V., Varrault, G., 2015. Influence of effluent organic matter on
643 copper speciation and bioavailability in rivers under strong urban pressure. Environ. Sci. Pollut.
644 Res. 22, 19461–19472. https://doi.org/10.1007/s11356-015-5110-6

645 NF ISO 11265, 1994. Qualité du sol—détermination de la conductivité électrique spécifique,
646 AFNOR.

647 Parikh, S.J., Goyne, K.W., Margenot, A.J., Calderón, F.J., 2014. Soil Chemical Insights
648 Provided Through Vibrational Spectroscopy, in: Advances in Agronomy. pp. 1–148.
649 https://doi.org/10.1016/B978-0-12-800132-5.00001-8

650 Prasad, M.B.K., Ramanathan, A.L., Shrivastav, S.K., Anshumali, Saxena, R., 2006. Metal
651 fractionation studies in surfacial and core sediments in the Achankovil River Basin in India.
652 Environ. Monit. Assess. 121, 77–102. https://doi.org/10.1007/s10661-005-9108-2

653 Quenea, K., Lamy, I., Winterton, P., Bermond, A., Dumat, C., 2009. Interactions between
654 metals and soil organic matter in various particle size fractions of soil contaminated with waste
655 water. Geoderma 149, 217–223. https://doi.org/10.1016/j.geoderma.2008.11.037

656 Schuttlefield, J.D., Cox, D., Grassian, V.H., 2007. An investigation of water uptake on clays
657 minerals using ATR-FTIR spectroscopy coupled with quartz crystal microbalance
658 measurements. J. Geophys. Res. 112, D21303. https://doi.org/10.1029/2007JD008973

659 Shi, H., Li, Q., Chen, W., Cai, P., Huang, Q., 2018. Distribution and mobility of exogenous
660 copper as influenced by aging and components interactions in three Chinese soils. Environ. Sci.
661 Pollut. Res. 25, 10771–10781. https://doi.org/10.1007/s11356-018-1288-8

662 Thien, S.J., Graveel, J.G., 2003. Laboratory Manual for Soil Science: Agricultural and
663 Environmental Principles, 8th ed. McGraw-Hill Publishing Company, Boston, MA.

664 Wazne, M., Korfali, S., 2016. Spatial and temporal assessment of metal pollution in the
665 sediments of the Qaraoun reservoir, Lebanon. Environ. Sci. Pollut. Res. 23, 7603–7614.
666 https://doi.org/10.1007/s11356-015-6022-1